High-pressure behavior of tetragonal barium carbodiimide, BaNCN

Yuji Masubuchi*[1], Suzuka Miyazaki[2], Peng Song[3], Takafumi Yamamoto[4], Kosuke Nakano[5], Kenta Hongo[5], Ryo Maezono[3]

Affiliations:

1. Faculty of Engineering, Hokkaido University, N13 W8, Kita-ku, Sapporo 060-8628, Japan

2. Graduate School of Chemical Sciences and Engineering, Hokkaido University, N13 W8, Kita-ku, Sapporo 060-8628, Japan

3. School of Information Science, JAIST, Asahidai 1-1, Nomi, Ishikawa 923-1292, Japan

4. Laboratory for Materials and Structures, Tokyo Institute of Technology, Yokohama 226-8503, Japan

5. Research Center for Advanced Computing Infrastructure, JAIST, Asahidai 1-1, Nomi, Ishikawa 923-1292, Japan

*Corresponding author: Yuji Masubuchi; Faculty of Engineering, Hokkaido University, N13 W8, Kita-ku, Sapporo 060-8628, Japan; Tel: +81-(0)11-706-6742; E-mail: yuji-mas@eng.hokudai.ac.jp

Abstract

The high-pressure behavior of tetragonal barium carbodiimide (BaNCN) was investigated by in-situ high-pressure X-ray diffraction measurements and first-principles theoretical calculations. No phase transition or decomposition of tetragonal BaNCN was observed during compression to 6.0 GPa and subsequent decompression to ambient pressure. The bulk modulus estimated from the unit cell volume with respect to the applied pressure was 69(2) GPa, which is comparable to that estimated by first-principles calculations. The

theoretical calculations indicate that contraction of the Ba-N bond length has a crucial effect on the volume change in response to pressure, whereas the C-N bonds in the NCN^{2-} anions remain robust against the change in pressure.

Keywords

Carbodiimide; Crystal structure; high-pressure; X-ray diffraction; Density functional theory

Introduction

Metal carbodiimides are interesting inorganic compounds that consist of a dumbbell-like $N=C=N^{2-}$ anionic group, which can replace oxide anions having the same negative charge. The two terminal N atoms are bonded with cations via an isolated negative charge on the N atoms. These compounds have been studied for their electrochemical activities in Li and Na ion batteries, as photocatalysts for water oxidation, and as phosphor materials when doped with photoluminescence elements [1-13]. Our group has recently reported the synthesis of tetragonal BaNCN by the ammonolysis reaction of $BaCO_3$ [14]. The crystal structure is related to the CsCl-type structure for Ba^{2+} and NCN^{2-} ions, where Ba^{2+} is coordinated with 8 nitrogen atoms to form a square antiprism polyhedron, as shown in Fig. 1. Divalent Eu-doped tetragonal BaNCN shows strong red luminescence under blue light irradiation because of the $4f^65d^1 \rightarrow 4f^7$ transition in Eu^{2+}. The peak wavelength is blue-shifted from 680 nm at 80 K to 640 nm at 500 K. The BaNCN host lattice has large thermal expansion coefficients, and the crystal field splitting of the 5d levels of the Eu^{2+} ions varies depending on the bond length. Modulation of the crystal field strength by compression of the BaNCN structure has been studied by photoluminescence (PL) analysis under high static pressures up to 5.34 GPa [15]. The wavelength of the PL was strongly red-shifted at a rate of 19 nm/GPa. This shift rate is almost 50 times larger than that for the ruby R_1-line, which is used as a pressure sensor in high-pressure experiments. The high-pressure behavior of tetragonal BaNCN has not been examined to date, but it is expected to exhibit a small bulk modulus because of the wide change in the PL wavelength of the BaNCN:Eu^{2+} phosphor under a high static pressure.

The high-pressure behavior of metal cyanamides, which contain asymmetric $N\text{-}C\equiv N^{2-}$ anions characterized by two different N-C bonds [16], has only been reported for PbNCN and HgNCN [17,18]. Their bulk moduli has been estimated to be 19 GPa and 38.5 GPa, respectively. Anisotropic compression was investigated in orthorhombic PbNCN because of the dumbbell-like structure of the NCN^{2-} anions. The smallest change at pressures less than 6.5 GPa was observed in the lattice parameter, *a*. The NCN^{2-} anions are almost parallel to

the *a*-axis in PbNCN. Compressibilities approximately 4 times and 9 times larger were observed along the *b*- and *c*-axes, respectively. Large compressibility has also been suggested by density functional theory (DFT) calculations for $Si(CN_2)_2$ containing the NCN^{2-} moiety [19]. Low-compressibility and super-hard properties of C-N binary compounds have been proposed on the basis of theoretical calculations and experimental studies [20-24]. The low compressibility of the C-N bond in the NCN^{2-} moiety has also been studied for PbNCN by DFT calculations. Zero linear compressibility of *M*NCN (*M*=Ca, Fe, Li_2) was suggested along the crystalline axis parallel to the linear NCN^{2-} anion combined with NM_x polyhedra because of robust C-N bonds and flexible N-*M* bonds and *M*-N-*M* angles estimated for their theoretical crystal structures [25]. The high-pressure behavior of both metal-N and C-N bonds should be examined to investigate the high-pressure compressibility of metal carbodiimides. Therefore, both X-ray diffraction (XRD) measurements and theoretical calculations are required to investigate the high-pressure behavior of NCN^{2-} carbodiimide anions bonding with Ba^{2+} cations in BaNCN because they have small X-ray scattering factors compared with that for the heavy Ba cation.

Understanding the relationship between the crystal structure and physical properties is essential for the successful development of materials. Investigating the pressure-dependent PL wavelength for the BaNCN:Eu^{2+} phosphor requires detailed knowledge of its local structure. In the present study, high-pressure synchrotron X-ray diffraction (SXRD) measurements were performed to study the crystal structure of tetragonal BaNCN under high pressures. The local structure around the Ba atoms is difficult to analyze using conventional XRD because of the large contrast in the X-ray scattering factors between heavy Ba and light C/N elements. The details of the crystal structure under pressure are also discussed with respect to DFT calculations.

Experimental procedure

Methods: Tetragonal BaNCN was prepared by the ammonolysis reaction of $BaCO_3$ (99.9%,

Fujifilm Wako Pure Chemical), similar to the preparation reported in our previous work [14]. $BaCO_3$ in an alumina boat was nitrided under a 100 mL/min NH_3 (99.9%, Sumitomo Seika) flow at 900 °C for 15 h. After the nitridation reaction, the product was transferred into a glove box filled with dry Ar. The crystalline phases of the product were evaluated with XRD analysis (Ultima-IV, Rigaku) using Cu $K\alpha$ radiation. Powder SXRD experiments under static high pressures up to 6.0 GPa were performed at room temperature for tetragonal BaNCN using the NE1A synchrotron beam line of the Photon Factory, Advanced Ring for Pulse X-ray (PF-AR) at the High Energy Accelerator Research Organization (KEK). A powder sample was loaded into a 200 μm hole of pre-indented rhenium gaskets in a diamond anvil cell (DAC) with a 600 μm culet. Daphne oil 7373 was used as a pressure transmitting medium. The fluorescence shift of the ruby R_1-line was used to calibrate the pressure. Two ruby chips were placed inside the hole at different distances from the center to estimate the pressure distribution along the sample. The pressure gradient increased with increasing pressure, but did not exceed 0.2 GPa at maximum pressure. The incident X-ray beam was monochromatized to a wavelength of 0.4175 Å and collimated to a diameter of approximately 60 μm. The SXRD data were analyzed using the RIETAN-FP program to estimate the lattice parameters [26]. Crystal structure images were drawn using the VESTA program [27].

Computational study: The structural properties of BaNCN were calculated using the DFT method, as implemented in the Vienna Ab initio Simulation Package (VASP) [28-31]. The generalized gradient approximation (GGA) of the Perdew–Burke–Ernzerhof (PBE) was used to describe the exchange-correlation functional [32]. The electron-ion interaction was described by the projector-augmented-wave (PAW) method with 5s5p6s, 2s2p and 2s2p as valence electrons for Ba, C, and N, respectively. The smallest allowed spacing between the k-points in the Brillouin zone was set to be 0.2 $Å^{-1}$ with a cutoff energy of 600 eV. The conjugate gradient algorithm, which was implemented in the VASP code, was used to explore the crystal structure at high pressures [33]. Selected bond lengths were estimated from the structural parameters reproduced by theoretical calculations for each pressure. The bulk

modulus was then obtained by fitting the total energy and volume data to the third order Birch-Murnaghan equation of state (EOS) [34].

Results and discussion

Figure 2 shows SXRD patterns for tetragonal BaNCN during compression to 6.0 GPa and decompression to ambient pressure. No additional peak appeared during the high-pressure experiment. No decomposition or phase transition was observed in this pressure range. The SXRD pattern at 0 GPa (ambient pressure) after the compression/decompression experiment returned to the initial pattern (Fig. S1 in the electronic supplementary information) observed before the high-pressure experiment [14]. Peak broadening and a change in the relative intensity of the diffraction lines in response to the change of pressure were caused by sample displacement or small pressure variation on the sample during the high-pressure experiment using the DAC technique. The Eu-doped BaNCN phosphor showed a red-shift in its PL wavelength from 660 nm at ambient pressure to 700 nm at 5.4 GPa. The PL wavelength returned to the initial wavelength after the compression and decompression experiment. Good reproducibility of the PL wavelength indicated that the tetragonal BaNCN host lattice recovered to that at ambient pressure after experiments at pressures as high as 5.4 GPa [15]. Lattice parameters were estimated from the SXRD patterns; however, because of the small X-ray scattering factors for C and N compared with that for heavy Ba, and because of the preferred orientation of the grains used in the SXRD measurement, structural parameters such as the N position and displacement factors were not analyzed. The estimated lattice parameters are depicted in Figure 3. The BaNCN sample has lattice parameters of a = 6.0139(5) Å and c = 7.1799(7) Å at 0 GPa after decompression to ambient pressure. The values are almost consistent with those reported for tetragonal BaNCN (a = 6.0249(4) Å and c = 7.1924(5) Å) [14]. The lattice parameters for tetragonal BaNCN decreased with increasing pressure and the lattice compressibilities at pressures up to 6 GPa were approximately 2.0% for the *a*-axis and 3.4% for the *c*-axis (Fig. 4(a)). Preferred compression along the *c*-axis was

also observed in the temperature dependence of the lattice parameters [14]. The thermal expansion coefficient for the *c*-axis was $\alpha_c = 2.3\times10^{-5}$ K^{-1}, which was larger than that for the *a*-axis, $\alpha_a = 1.5\times10^{-5}$ K^{-1}. The preferred shrinkage along the *c*-axis, both at high pressure and at low temperature, may be closely related to the stacking structure of Ba^{2+} and NCN^{2-} ions along the *c*-axis. NCN^{2-} ions align perpendicular to the *c*-axis and stack alternately with the Ba^{2+} layers, as shown in Fig. 1(a). Anisotropic compression was also observed in PbNCN [17].

The bulk modulus for the BaNCN was estimated to be 69(2) GPa by Birch-Murnaghan fitting of the lattice volume dependence on the pressure [35]. This value is much lower than that for Ba-related compounds such as $BaTiO_3$ (bulk modulus: 135 GPa) and $BaSiO_3$ (200 GPa), and those for traditional ceramics such as *a*-Al_2O_3 (253 GPa) and Si_3N_4 (228 GPa) [36-39] but is comparable to that for the the binary barium oxide BaO (77.5 GPa) with a rock-salt type structure [40]. Metal carbodiimides and cyanamides have been reported to exhibit large compressibility. The high-pressure behavior of metal cyanamide containing $N\text{-}C\equiv N^{2-}$ anions has been studied for PbNCN and HgNCN, and their bulk moduli were found to be 19 GPa and 38.5 GPa, respectively [17,18]. Anisotropic compressibility was observed in PbNCN. The compressibility perpendicular to the NCN^{2-} moieties was several times larger than that parallel to the dumbbell-like anions.

DFT calculations were performed to investigate the pressure dependence of the tetragonal BaNCN crystal structure. The calculated lattice parameters were normalized with respect to the values at 0 GPa, and the results are shown in Fig. 4(b). The lattice compressibility up to 6 GPa agreed well with the observed values shown in Fig. 4(a) and Table 1. The differences between the experimental and theoretical lattice parameters are below the typical errors of 1-2% using the GGA-PBE functional [41]. The preferred shrinkage along the *c*-axis compared with that along the *a*-axis and the compressibility at pressures up to 6 GPa were reproduced well by the DFT calculations. The dependence of the total energy of the tetragonal BaNCN on the unit cell volume was fitted with the third order Birch-Murnaghan EOS, as shown in Fig.

5, and the bulk modulus was estimated to be 68 GPa, in good agreement with the experimental value determined from the high-pressure SXRD patterns.

Details of the calculated crystal structure are summarized in Table 1. The bond lengths for Ba-N and C-N at 0 GPa were 2.936 Å and 1.242 Å, respectively, which agree well with the reported values shown in Table 1. The C-N bond lengths are almost consistent with the C-N double bond in metal carbodiimides, i.e., 1.19-1.24 Å [42]. In the DFT calculation, the bonding nature between C and N in the NCN^{2-} moiety was restricted to a symmetrical and straight tri-atomic molecular anion, $N=C=N^{2-}$. Asymmetric bonds consisting of single and triple bonds that appear in a cyanamide anion $N-C\equiv N^{2-}$ were not considered in this research. The energy difference between $N=C=N^{2-}$ and $N-C\equiv N^{2-}$ triatomic anions is considered to be small and the difference in their stiffness was excluded in Ref. 17. Fourier transform infrared (FT-IR) spectroscopy of the BaNCN under high pressure will facilitate understanding of the high-pressure behavior of the anions.

Figure 6 shows that the compressibility of the Ba-N bond was 3.2% at a pressure of 6 GPa, whereas that of the C-N bond was 0.4%. The bond angles around the Ba^{2-} and NCN^{2-} anions changed within 1° when BaNCN was compressed from 0 to 6 GPa. The $Ba\text{-}N_8$ square antiprism polyhedron was substantially compressed but not distorted with increasing pressure, whereas the NCN anion was not. The stiffness of the C-N bond has been reported for PbNCN [17] and theoretical *M*NCN structures [25].

Carbodiimide (NCN^{2-}) anions are pseudo-oxide anions, because they can replace O^{2-} anions having same negative charge. Rock-salt type BaO exhibits relatively high compressibility and a bulk modulus of 77.5 GPa. Analogous with BaO, BaNCN exhibits high compressibility that originates from contraction of the Ba-N bond with increasing pressure, although the NCN^{2-} anion is rigid, similar to PbNCN. The red-shift in the PL wavelength of the BaNCN:Eu^{2+} phosphor under increasing pressure is attributed to the large contraction of the bond around Ba^{2+}, which is partially occupied with doped Eu^{2+}. The crystal field strength is proportional to R^{-5}, where R is the bond length [43]. Downward of the 5d states, a change

in the $4f^6 5d^1 \rightarrow 4f^7$ transition occurs, which results in a substantial red-shift of the PL wavelength.

Conclusion

The high compressibility of tetragonal BaNCN was examined by in situ high pressure SXRD and DFT calculations. Tetragonal BaNCN has a bulk modulus of 69(2) GPa, which is similar to that for rock-salt type BaO. DFT calculations showed a large contribution of Ba-N bond contraction to the lattice volume compression and rigid NCN anionic groups in the BaNCN lattice. Metal carbodiimides can have both soft chemical bonds around the metal cations and rigid NCN^{2-} anions under high pressure, leasing to the possibility of new and unique high-pressure chemistry.

Declaration of competing interests

The authors declare that they have no known competing financial interests or personal relationships that could have appeared to influence the work reported in this paper.

Acknowledgement

This work was supported in part by Grants-in-Aid for Scientific Research on Innovative Areas “Mixed Anion” (Nos. JP16H06438, JP16H06439, JP16H06440, and 19H04692) from the Japan Society for the Promotion of Science (JSPS). High-pressure synchrotron radiation experiments were performed under the approval of the Photon Factory Program Advisory Committee (No. 2019G021). The high-pressure XRD experiments were supported by the Visiting Researcher's Program of the Institute for Solid State Physics, the University of Tokyo. The authors thank Daisuke Nishio-Hamane and Hirotada Gotou for their support with the DAC preparation.

References

[1] M.T. Sougrati, A. Darwiche, X. Liu, A. Mahmoud, R.P. Hermann, S. Jouen, L. Monconduit, R. Dronskowski, L. Stievano, Transition-metal carbodiimides as molecular negative electrode materials for lithium- and sodium-ion batteries with excellent cycling properties, Angew. Chem. Int. Ed. 55 (2016) 5090–5095.

[2] A. Eguia-Barrio, E. Castillo-Matrinez, X. Liu, R. Dronskowski, M. Armand, T. Rojo, Carbodiimides: new materials applied as anode electrodes for sodium and lithium ion batteries, J. Mater. Chem. A 4 (2016) 1608–1611.

[3] A. Eguia-Barrio, E. Castillo-Martínez, F. Klein, R. Pinedo, L. Lezama, J. Janek, P. Adelhelm, T. Rojo, Electrochemical performance of CuNCN for sodium ion batteries and comparison with ZnNCN and lithium ion batteries, J. Power Sources 367 (2017) 130–137.

[4] Q. Liua, Y. Liua, G. Dai, L. Tian, J. Xua, G. Zhao, Na Zhang, Y. Fang, Size controllable synthesis of hierarchical copper carbodiimide microcrystals and their pronounced photoelectric response under visible light, Appl. Surf. Sci. 357 (2015) 745–749.

[5] D. Ressnig, M. Shalom, J. Patscheider, R. More, F. Evangelisti, M. Antonietti, G.R. Patzke, Photochemical and electrocatalytic water oxidation activity of cobalt carbodiimide, J. Mater. Chem. A 3 (2015) 5072–5082.

[6] S. Yuan, Y. Yang, F. Chevire, F. Tessier, X. Zhang, G. Chen, Photoluminescence of Eu^{2+}-doped strontium cyanamide: a novel host lattice for Eu^{2+}, J. Am. Ceram. Soc. 93 (2010) 3052–3055.

[7] M. Krings, G. Montana, R. Dronskowski, C. Wickleder, Alpha-SrNCN:Eu^{2+} - a novel efficient orange-emitting phosphor, Chem. Mater. 23 (2011) 1694–1699.

[8] J. Sindlinger, J. Glaser, H. Bettentrup, T. Justel, H.J. Meyer, Synthesis of $Y_2O_2(CN_2)$ and luminescence properties of $Y_2O_2(CN_2)$:Eu, Z. Anorg. Allg. Chem. 633 (2007) 1686–1690.

[9] J. Glaser, L. Unverfehrt, H. Bettentrup, G. Heymann, H. Huppertz, T. Justel, H.J. Meyer, Crystal structures, phase-transition, and photoluminescence of rare earth carbodiimides, Inorg. Chem. 47 (2008) 10455–10460.

[10] E. Leysour de Rohello, F. Bour, Y. Suffren, O. Merdrignac-Conanec, O. Guillou, F. Chevire, Synthesis and photoluminescence properties of Mn^{2+} doped $ZnCN_2$ phosphor, Open Ceram. 7 (2021) 100157/1-9.

[11] W. He, H. Li, B. Long, M. Xiao, T. Song, X. Wang, Y. Tong, One-step synthesis of ZnNCN nanoparticles with adjustable composition for an advanced anode in lithium ion battery, ACS Appl. Energy Mater. 4 (2021) 4290-4296.

[12] C. Braun, L. Mereacre, W. Hua, T. Sturzer, I. Ponomarev, P. Kroll, A. Slabon, Z. Chen, Y. Damour, X. Rocquefelte, J.-F. Halet, S. Indris, $SnCN_2$: a carbodiimide with an innovative approach for energy storage systems and phosphors in modern LED Technology, ChemElectroChem 7 (2020) 4550-4561.

[13] J. Li, R. Wang, P. Guo, X. Liu, Y. Hu, Z. Xu, Y. Liu, L. Cao, J. Huang, K. Kajiyoshi, Realizing fast charge diffusion in oriented iron carbodiimide structure for high-rate sodium-ion storage performance, ACS Nano, 15 (2021) 6410-6419.

[14] Y. Masubuchi, S. Nishitani, A. Hosono, Y. Kitagawa, J. Ueda, S. Tanabe, H. Yamane, M. Higuchi, S. Kikkawa, Red-emission over a wide range of wavelength at various temperatures from tetragonal $BaCN_2$:Eu^{2+}, J. Mater. Chem. C 6 (2018) 6370–6377.

[15] Y. Masubuchi, S. Nishitani, S. Miyazaki, H. Hua, J. Ueda, M. Higuchi, S. Tanabe, Large red-shift of luminescence from $BaCN_2$:Eu^{2+} red phosphor under high pressure, Appl. Phys. Exp. 13 (2020), 042009/1-3.

[16] X. Liu, P. Muller, P. Kroll, R. Dronskowski, Synthesis, structure determination, and quantum-chemical characterization of an alternate HgNCN polymorph, Inorg. Chem. 41 (2002) 4259-4265.

[17] A. Moller, P. M. Konze, R. Dronskowski, High-pressure behavior of lead cyanamide PbNCN, Z. Anorg. Allg. Chem., 644 (2018) 1881-1885.

[18] H. Liu, W. Klein, H. Bender, M. Jansen, High pressure behavior of mercury cyanamide $HgCN_2$, Z. Anorg. Allg. Chem. 628 (2002) 4-6.

[19] P. Kroll, R. Riedel, R. Hoffmann, Silylated carbodiimides in molecular and extended

structures, Phys. Rev. B, 60 (1999) 3126-3139.

[20] A. Y. Liu, M. L. Cohen, Prediction of new low compressibility solids, Science, 245 (1989) 841-842.

[21] D. M. Teter, R. J. Hemley, Low-compressibility carbon nitrides, Science, 271, (1996) 53-55.

[22] S. Muhl, J. M. Mendez, A review of the preparation of carbon nitride films, Diamond Relat. Mater., 8 (1999) 1809-1830.

[23] H. M. Ma, X. P. Jia, P. W. Zhu, W. L. Guo, X. B. Guo, Y. D. Wang, S. Q. Li, G. T. Zou, G. Zhang, P. Bex, High-pressure pyrolysis study of $C_3N_6H_6$: a route to preparing bulk C_3N_4, J. Phys. Condens. Matter, 14 (2002) 11269-11273.

[24] V. N. Khabashesku, J. L. Zimmerman, J. L. Margrave, Powder synthesis and characterization of amorphous carbon nitride, Chem. Mater., 12 (2000) 3264-3270.

[25] Q. Zeng, W. Qiu, J. Hao, K. Wang, Y. Li, Tunable zero linear compressibility under a rational designed mechanism of modular “dumbbell”: a density functional theory study, ACS Mater. Lett. 4 (2022) 541-547.

[26] F. Izumi, K. Momma, Three-dimensional visualization in powder diffraction, Solid State Phenom., 130 (2007) 15-20.

[27] K. Momma, F. Izumi, VESTA: a three-dimensional visualization system for electronic and structural analysis, J. Appl. Crystallogr., 41 (2008) 653-658.

[28] G. Kresse, J. Hafner, Ab initio molecular dynamics for liquid metals, Phys. Rev. B, 47 (1993) 558-561.

[29] G. Kresse, J. Hafner, Ab initio molecular-dynamics simulation of the liquid-metal–amorphous-semiconductor transition in germanium, Phys. Rev. B, 49 (1994) 14251-14269.

[30] G. Kresse, J. Furthmuller, Efficiency of ab-initio total energy calculations for metals and semiconductors using a plane-wave basis set, Comput. Mater. Sci., 6 (1996) 15-50.

[31] G. Kresse, J. Furthmuller, Efficient iterative schemes for ab initio total-energy calculations using a plane-wave basis set, Phys. Rev. B, 54 (1996) 11169-11186.

[32] J. P. Perdew, K. Burke, M. Ernzerhof, Generalized gradient approximation made simple, Phys. Rev. Lett., 77 (1996) 3865-3868.

[33] M. R. Hestenes E. Stiefel, Methods of conjugate gradients for solving linear systems, J. Res. Natl. Bur. Stand., 49 (1952) 409-436.

[34] F. Birch, Finite elastic strain of cubic crystals. Phys. Rev., 71 (1947) 809-824.

[35] F. Birch, The effect of pressure upon the elastic parameters of isotropic solids, according to Murnaghan's theory of finite strain, J. Appl. Phys., 9 (1938) 279-288.

[36] P. Pruzan, D. Gourdain, J. C. Chervin, B. Canny, B. Couzinet, M. Hanfland, Equation of state of $BaTiO_3$ and $KNbO_3$ at room temperature up to 30 GPa, Solid State Commun., 123 (2002) 21-26.

[37] Q. Mahmood, M. Hassan, S. H. A. Ahmad, A. Shahid, A. Laref, Study of optoelectronic and thermoelectric properties of $BaSiO_3$ perovskite under moderate pressure for energy renewable devices applications, J. Phys. Chem. Solid, 120 (2018) 87-95.

[38] P. Richet, J. A. Xu, H. K. Mao, Quasi-hydrostatic compression of ruby to 500 Kbar, Phys. Chem. Mater., 16 (1988) 207-2011.

[39] M. B. Kruger, J. H. Nguyen, Y. M. Li, W. A. Caldwell, M. H. Manghnani, R. Jeanloz, Equation of state of a-Si_3N_4, Phys. Rev. B, 55 (1997) 3456-3460.

[40] K. O. Park, J. M. Sivertsen, Temperature dependence of the bulk modulus of BaO single crystals. J. Am. Ceram. Soc., 60 (1977) 537-538.

[41] L. He, F. Liu, G. Hautier, M. J. T. Oliveira, M. A. L. Marques, F. D. Vila, J. J. Rehr, G.-M. Rignanese, A. Zhou, Accuracy of generalized gradient approximation functionals for density-functional perturbation theory calculations, Phys. Rev. B, 89, (2014) 064305.

[42] U. Berger, W. Schnick, Synthesis, crystal structures, and vibrational spectroscopic properties of $MgCN_2$, $SrCN_2$, and $BaCN_2$, J. Alloys Compd., 206 (1994) 179-184.

[43] P. D. Rack, P. H. Holloway, The structure, device physics, and material properties of thin film electroluminescence displays, Mater. Sci. Eng., R21 (1998) 171-219.

Figure captions

Figure 1, Crystal structure of tetragonal barium cyanamide (BaNCN) viewed along (a) the *a*-axis, (b) the *c*-axis, and (c) a $Ba(NCN)_8$ polyhedron. Green, brown, and gray spheres correspond to Ba, C and N, respectively.

Figure 2, XRD patterns for tetragonal BaNCN during compression and decompression.

Figure 3, Pressure dependence of lattice parameters and unit cell volume for tetragonal BaNCN. The filled red triangles and blue circles indicate the *a*-axis and *c*-axis lattice parameters, respectively, observed during the compression. The open symbols indicate the values obtained during the decompression. The reference values reported in our previous paper [14] are shown as red, blue, and black squares for *a*-axis, *c*-axis, and cell volume, respectively.

Figure 4, (a) Normalized lattice parameters estimated from the SXRD patterns and (b) dependence of the calculated lattice parameters on the pressure. The values are normalized with respect to those at ambient pressure (0 GPa). Red triangles and blue circles correspond to the *a*-axis and *c*-axis lattice parameters, respectively.

Figure 5, Birch-Murnaghan EOS fitting (broken line) for the calculated lattice energy (red circles) as a function of the unit cell volume.

Figure 6, (a) Theoretical bond distances and (b) the normalized bond lengths. The blue circles and red triangles correspond to the bond distances of Ba-N and C-N, respectively.

Figure 1

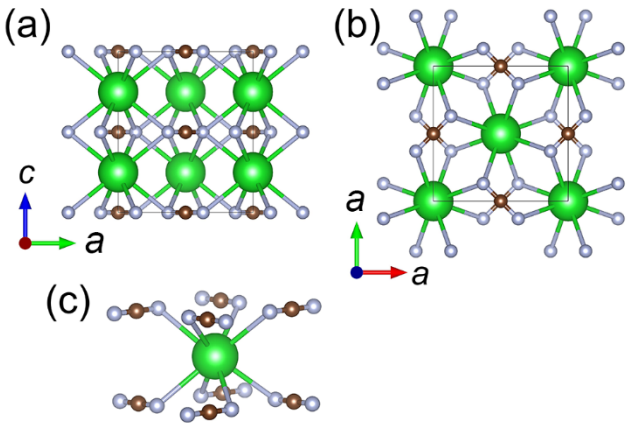

Figure 1, Crystal structure of tetragonal barium cyanamide (BaNCN) viewed along (a) the *a*-axis, (b) the *c*-axis, and (c) a $Ba(NCN)_8$ polyhedron. Green, brown, and gray spheres correspond to Ba, C and N, respectively.

Figure 2

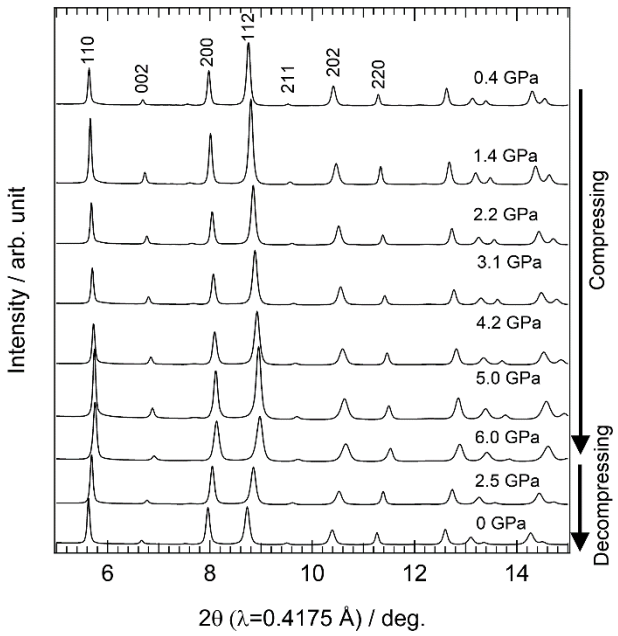

Figure 2, XRD patterns for tetragonal BaNCN during compression and decompression.

Figure 3

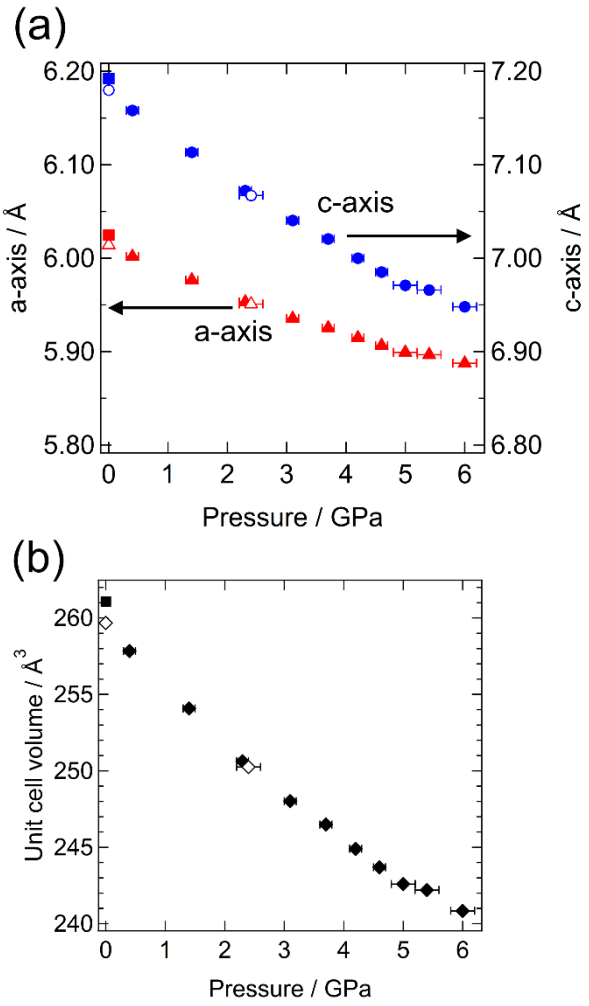

Figure 3, Pressure dependence of lattice parameters and unit cell volume for tetragonal BaNCN. The filled red triangles and blue circles indicate the *a*-axis and *c*-axis lattice parameters, respectively, observed during the compression. The open symbols indicate the values obtained during the decompression. The reference values reported in our previous paper [14] are shown as red, blue, and black squares for *a*-axis, *c*-axis, and cell volume, respectively.

Figure 4

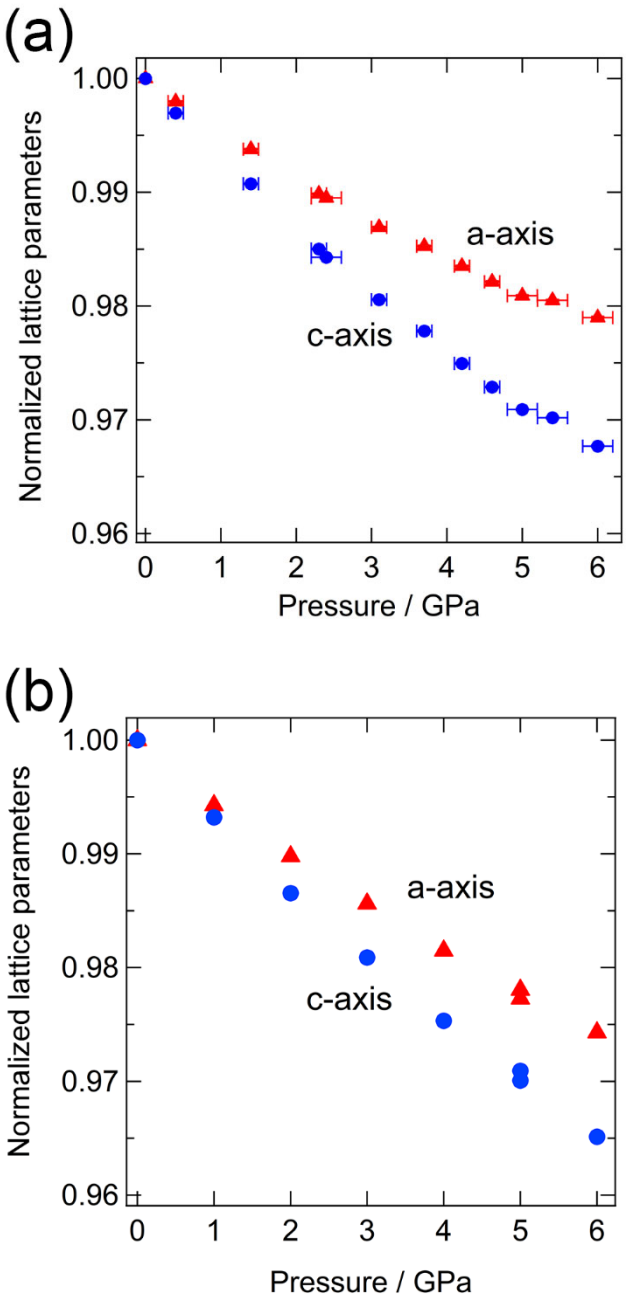

Figure 4, (a) Normalized lattice parameters estimated from the SXRD patterns and (b) dependence of the calculated lattice parameters on the pressure. The values are normalized with respect to those at ambient pressure (0 GPa). Red triangles and blue circles correspond to the *a*-axis and *c*-axis lattice parameters, respectively.

Figure 5

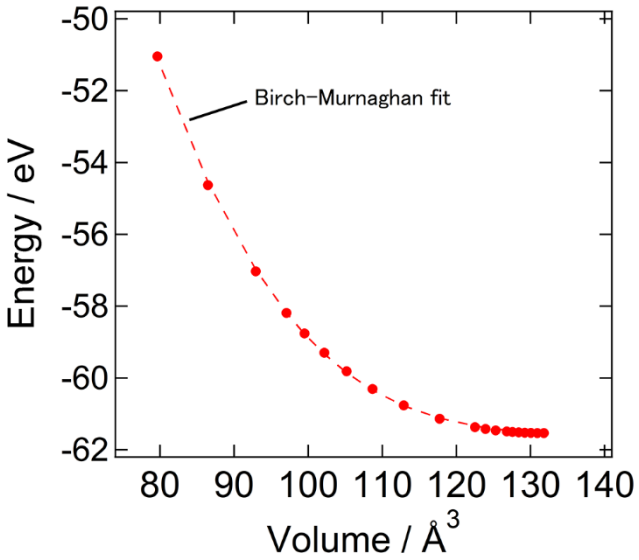

Figure 5, Birch-Murnaghan EOS fitting (broken line) for the calculated lattice energy (red circles) as a function of the unit cell volume.

Figure 6

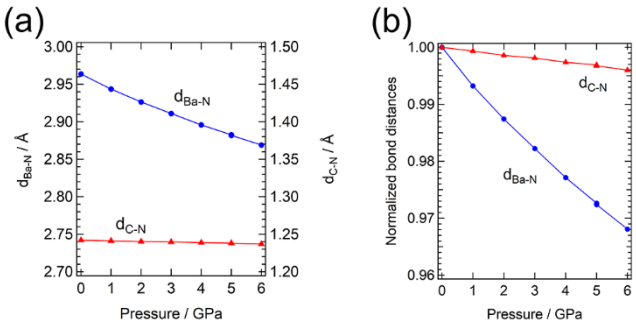

Figure 6, (a) Theoretical bond distances and (b) the normalized bond lengths. The blue circles and red triangles correspond to the bond distances of Ba-N and C-N, respectively.

Table 1 Experimental lattice parameters estimated from SXRD patterns at 0 and 6 GPa, and theoretical lattice parameters. The reference values were obtained from the single crystal XRD data reported in Ref. 14.

Parameters	Experimental		Theoretical		Ref. [14]
	0 GPa	6 GPa	0 GPa	6 GPa	
a / Å	6.0139(5)	5.8876(6)	6.08815	5.9317	6.0249(4)
c / Å	7.1799(7)	6.9479(8)	7.28923	7.0351	7.1924(5)
Volume, V / $Å^3$	259.68(4)	240.84(5)	270.2	247.5	261.08(4)
d_{Ba-N} / Å	-	-	2.9636	2.8690	2.928(5)
d_{C-N} / Å	-	-	1.2420	1.2380	1.233(7)